

On the definitions and simulations of vibrational heat transport in nanojunctions

Na'im Kalantar,¹ Bijay Kumar Agarwalla,² and Dvira Segal^{3,4,*}

¹*Chemical Physics Theory Group, Department of Chemistry,
University of Toronto, 80 Saint George St., Toronto, Ontario, Canada M5S 3H6*

²*Department of Physics, Dr. Homi Bhabha Road,
Indian Institute of Science Education and Research, Pune, India 411008*

³*Chemical Physics Theory Group, Department of Chemistry and Centre for Quantum Information and Quantum Control,
University of Toronto, 80 Saint George St., Toronto, Ontario, Canada M5S 3H6*

⁴*Department of Physics, University of Toronto, Toronto, Ontario, Canada M5S 1A7*

(Dated: August 31, 2020)

Thermal transport through nanosystems is central to numerous processes in chemistry, material sciences, electrical and mechanical engineering, with classical molecular dynamics as the key simulation tool. Here we focus on thermal junctions with a molecule bridging two solids that are maintained at different temperatures. The classical steady state heat current in this system can be simulated in different ways, either at the interfaces with the solids, which are represented by thermostats, or between atoms within the conducting molecule. We show that while the latter, intramolecular definition feasibly converges to the correct limit, the molecule-thermostat interface definition is more challenging to converge to the correct result. The problem with the interface definition is demonstrated by simulating heat transport in harmonic and anharmonic one-dimensional chains illustrating unphysical effects such as thermal rectification in harmonic junctions.

I. INTRODUCTION

Classical simulations of heat transfer through networks of beads and springs had played a crucial role in the development of nonlinear science^{1,2}, leading e.g. to the discovery of integrable systems with solitons as a prime example. Fundamentally, molecular dynamics simulations of vibrational heat flow in molecules aid in understanding chemical reactivity and e.g. protein folding dynamics³. For applications, understanding thermal energy propagation, redistribution, and dissipation is essential for developing electronic, mechanical, thermal and thermoelectric devices, specifically organic-inorganic heterostructures⁴⁻¹⁰.

Chains of beads and springs coupled at the edges to solids that are maintained at fixed temperatures serve to model heat transport in low dimensional systems. Abundance of simulations have demonstrated rich and often *anomalous* heat transport phenomena in low dimensional systems, specifically in one-dimensional (1D) chains, compared to the behavior of macroscopic objects^{8,11-13}. Recent experiments probed the flow of vibrational energy (heat) in self-assembled monolayers of alkanes¹⁴⁻¹⁶, down to the single molecule junction^{17,18}. As well, experiments in solutions were performed based on pump-probe spectroscopy methods¹⁹. In junction experiments, the setup constitutes a linear (quasi 1D) molecule bridging two solids with the steady state heat current, or the thermal conductance as observables of interest.

In this work, we study the nonequilibrium steady state vibrational heat transport in 1D chains connected to solids at the boundaries, as depicted in Fig. 1. The solid contacts are emulated with thermostats; here we adopt Langevin baths. Such classical simulations have a long and rich history^{8,13,20}. Recent studies (i) continue to address the fundamental anomalous properties of heat

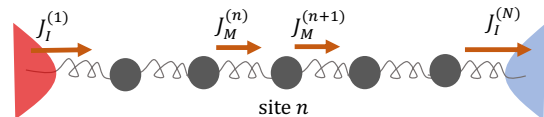


FIG. 1. Scheme of a vibrational heat transport junction. A molecular chain is attached to heat baths (solids) at the boundaries, with the baths emulated by Langevin thermostats. The intramolecular currents $J_M^{(n)}$ are calculated from Eq. (7). The interface currents (at the left and right contacts) are identified by $J_I^{(1)}$ and $J_I^{(N)}$, and are computed from Eq. (8). These expressions can be readily generalized beyond one-dimension to treat more complex structures.

conduction in periodic and disordered one-dimensional chains²¹⁻²⁷, (ii) recreate experimental setups to reveal transport mechanisms²⁸⁻³⁰, and (iii) provide guidelines for enhancing or suppressing the thermal conductance (oftentimes based on the harmonic force-field and using quantum scattering methods)³¹⁻³⁵. Naturally, one wonders: What problems in this field remain unresolved?

Here, we address a fundamental computational problem: How to efficiently and accurately simulate phononic heat transport in nonequilibrium situations as depicted in Fig. 1. This issue is far from being merely technical, since, as we show here, simulations that are only seemingly converged lead to faulty predictions of nonlinear functionality, and the violation of fundamental symmetries. This challenge, of converging simulations at low cost, boils down to making an adequate choice for the working definition of heat current in the system. In what follows we only focus on the contribution of the nuclei to thermal transport (referred to as vibrational or phononic conduction), and do not consider the additional electronic contribution.

We introduce two *equivalent*, intuitive definitions for

the steady state heat current in junctions: In the intramolecular (J_M) definition, the heat current is evaluated between particles *within* the conducting structure. In contrast, the interface (J_I) heat current is defined at the molecule-solid boundary, by calculating the net heat exchange between the solid (thermostat) and the molecule. While these two definitions are *mathematically* equivalent, we show that *computationally* the former (intramolecular expression) is superior: The interface definition suffers from a convergence problem, related to the challenge of achieving local energy equipartition at thermal equilibrium. In particular, the interface definition may lead to the erroneous identification of nonlinear phenomena in thermal transport, such as the (incorrect) observation of thermal rectification in harmonic chains.

It is quite interesting to note that contrasting the numerical problem, the interface definition is in fact advantageous in *formal-analytic* studies of anharmonic heat flow, full counting statistics, quantum heat transport, and more broadly quantum thermodynamics. For example, consider the problem of classical or quantum heat flow through an anharmonic structure. While the particles within the chain interact based on an anharmonic force field, the coupling between the molecular system and the bath is typically taken as a bilinear (harmonic) coupling form. As such, it is convenient to develop a formal expression for heat exchange *at the contact region*, rather than within the molecule—where the current needs to be defined in terms of high-order correlation functions⁹. Similarly, a full-counting statistics analysis of heat exchange, which follows the two-time measurement protocol is conveniently performed by considering the difference in energy content at the baths attached to the system³⁶.

As an additional example for the utility of the interface definition in formal methodologies, recall studies of quantum heat flow between a quantum system and a thermal bath. Given the ambiguity of a ‘heat current operator’³⁷, quantum heat exchange is calculated at the contact region: At weak system-bath coupling the time derivative of the expectation value, $d\langle H_S \rangle / dt$, yields the formal heat current expression $\text{Tr}[H_S D_K(\rho_S)]$ with $D_K(\rho_S)$ as the dissipator part of the dynamics due to the K th bath, which is responsible for heat exchange between the system and the K th reservoir; ρ_S is the density matrix of the system and H_S is the molecular (‘system’) Hamiltonian. The interface definition is indeed commonly employed in studies of quantum thermodynamics, even when approaching the strong system-bath coupling limit; some examples include Refs^{38,39}.

The interface and intramolecular definitions thus nicely complement: The interface definition is advantageous in formal studies of heat exchange, particularly in anharmonic systems. In contrast, in this paper we demonstrate that the intramolecular expression shows a better performance in numerical simulations, both in the frequency and time domain.

Interestingly, several recent studies revisited the defini-

tion of vibrational heat flux in low dimensional systems: In Ref.⁴⁰, the heat current was represented in two different ways following either a Lagrangian or an Eulerian approach, resulting in different microscopic definitions—that showed equivalent simulation results. In Ref.⁴¹, the impact of the thermostats (Langevin vs. Nose-Hoover) on thermal conduction was analyzed, and it was found that the Nose-Hoover approach lead to incorrect thermal rectification values. Our work further contributes to this endeavour, by comparing the intramolecular and interface definitions for the vibrational heat flux.

The paper is organized as follows. In Sec. II, we present the nanojunction and the Langevin equation of motion, as well as the intramolecular and interface definitions for phononic heat transport. In Sec. III, we focus on harmonic systems and present simulations in the frequency domain based on the Green’s function formalism. Molecular dynamics simulation are performed in Sec. IV, and we demonstrate the behavior of the different currents in both harmonic and anharmonic chains. We conclude in Sec. V.

II. MODEL AND METHOD

A. Langevin thermostats

We focus on one-dimensional molecular junctions as illustrated in Fig. 1. We write down the classical Hamiltonian and the corresponding classical equations of motion (EOM); a quantum description based on Heisenberg EOM directly follows⁸, but we do not describe it here. The classical Hamiltonian is

$$H = \sum_{n=1}^N \frac{p_n^2}{2m_n} + \sum_{n=2}^N V(x_n - x_{n-1}) + V_B(x_{N+1} - x_N - a) + V_B(x_1 - x_0 - a). \quad (1)$$

Here, x_n and p_n are the displacements and momenta, respectively, of the n th bead; x_0 and x_{N+1} are fixed points setting the boundaries. V is the intramolecular potential energy, and V_B (which could have the same functional form as V) is the potential energy between the atoms at the boundaries and the solids, setting the maximal extension of the molecule to $d = x_{N+1} - x_0$. Since x_0 and x_{N+1} are fixed, the potential energy V_B acts to confine sites 1 and N , respectively. One can generalize the model to include additional confining potential energy for all atoms.

To capture the solids at the left and right ends of the molecule, we further assume that the beads at the edges (1 and N) are coupled to independent heat baths (thermostats). This coupling is incorporated in the Langevin equation with a friction constants γ_n and stochastic forces $\xi_n(t)$; these terms are related through the fluctuation-dissipation relation. The beads can represent atoms or coarse-grained units in a more complex

system such as DNA. The classical EOMs for the displacements are

$$\begin{aligned} m_1 \ddot{x}_1 &= -\frac{\partial V}{\partial x_1} - \frac{\partial V_B}{\partial x_1} - \gamma_1 p_1(t) + \xi_1(t), \\ m_n \ddot{x}_n &= -\frac{\partial V}{\partial x_n}, \quad n = 2, 3, \dots, N-1, \\ m_N \ddot{x}_N &= -\frac{\partial V}{\partial x_N} - \frac{\partial V_B}{\partial x_N} - \gamma_N p_N(t) + \xi_N(t). \end{aligned} \quad (2)$$

The thermal-white noise is local and obeys the fluctuation-dissipation relation, $\langle \xi_p(t) \xi_l(t') \rangle = 2k_B T_p \gamma_p m_p \delta(t-t') \delta_{p,l}$. Here, k_B is the Boltzmann's constant. We emphasize that T_1 and T_N are not effective temperatures associated with sites 1 or N ; we do not make any assumptions on the notion of a local temperature. Rather, $T_{1,N}$ are the temperatures of the Langevin baths attached to these sites.

Specifically below we focus on harmonic chains with nearest-neighbor couplings,

$$V(x_n - x_{n-1}) = \frac{1}{2} k_{n,n-1} (x_n - x_{n-1} - a)^2. \quad (3)$$

The same form is assumed at the contacts for V_B . The EOM for e.g. the N th site then becomes

$$\begin{aligned} m_N \ddot{x}_N &= -k_{N,N-1} [x_N(t) - x_{N-1}(t) - a] \\ &+ k_{N,N+1} [x_{N+1}(t) - x_N(t) - a] - \gamma_N p_N(t) + \xi_N(t), \end{aligned} \quad (4)$$

where a is the equilibrium distance between neighboring particles.

B. Heat current definitions

Here, we derive the intramolecular and interface definitions of heat currents as used in Langevin molecular dynamics simulations^{8,20}. We focus on the steady state limit—once the effect of the initial conditions subside. Employing the EOM (2) for site N :

$$\begin{aligned} \langle p_N(t) \dot{p}_N(t) \rangle &= \frac{1}{2} \frac{d}{dt} \langle p_N(t)^2 \rangle \\ &= -\left\langle \frac{\partial V}{\partial x_N} p_N(t) \right\rangle - \left\langle \frac{\partial V_B}{\partial x_N} p_N(t) \right\rangle \\ &\quad - \gamma_N \langle p_N(t)^2 \rangle + \langle \xi_N(t) p_N(t) \rangle. \end{aligned} \quad (5)$$

In steady state, the local-site energy is constant. Here, the local energy at site N is the sum of kinetic energy plus the V_B confining potential. Using $\frac{d}{dt} \left(\frac{\langle p_N(t)^2 \rangle}{2m_N} \right) + \left\langle \frac{\partial V_B}{\partial x_N} v_N(t) \right\rangle = 0$, we get

$$-\left\langle \frac{\partial V}{\partial x_N} v_N(t) \right\rangle = \frac{\gamma_N}{m_N} \langle p_N(t)^2 \rangle - \frac{1}{m_N} \langle \xi_N(t) p_N(t) \rangle. \quad (6)$$

The average is done over initial conditions and by calculating heat exchange over a long time interval. $v_n = p_n/m_n$ is the velocity of the n th particle.

We identify the left hand side of Eq. (6) as the intramolecular current, $J_M^{(N)}$, flowing between site $N-1$ and site N . Since in steady state, $J_M^{(n)} = J_M^{(n+1)}$ we generally define the intramolecular current at site n as

$$J_M^{(n)} = \langle v_n F_n \rangle. \quad (7)$$

Here, $F_n = -V'(x_n - x_{n-1})$ is the force exerted from the $(n-1)$ th particle on the n th bead; derivative is taken with respect to the argument $x_n - x_{n-1}$.

Since $\langle v_n F_n \rangle = \langle v_n F_{n+1} \rangle$, It is common to calculate the intramolecular current based on an averaged two-bead expression by using either one of these expressions ($1 < n < N$), $J_M^{(n)} = \frac{1}{2} \langle v_n (F_{n+1} + F_n) \rangle = \frac{1}{2} \langle (v_n + v_{n-1}) F_n \rangle$.

Next, we identify the interface currents; $J_I^{(N)}$ is given by the right hand side of Eq. (6). By making use of the relationship $\langle p_n(t) \xi_l(t) \rangle = \gamma_n m_n k_B T_n \delta_{n,l}$ ⁴² we get

$$\begin{aligned} J_I^{(N)} &= \gamma_N \left(\frac{\langle p_N^2 \rangle}{m_N} - k_B T_N \right), \\ J_I^{(1)} &= -\gamma_1 \left(\frac{\langle p_1^2 \rangle}{m_1} - k_B T_1 \right), \end{aligned} \quad (8)$$

where similar considerations as in Eq. (6) resulted in $J_I^{(1)}$. The interface currents can be interpreted as the net heat exchange between the particles (1, N) and the attached thermostats, which are maintained at temperatures $T_{1,N}$. Note that the physical dimension of γ is inverse time. Particularly, at thermal equilibrium we expect that the interface current would vanish based on the principle of energy equipartition.

In our sign convention, positive current flows from left (site 1) to right (site N). The intramolecular current $J_M^{(n)}$ can be evaluated along the junction between every two sites, and we usually study it at the center of the chain. For simplicity, in what follows we set masses to one, $m_n = 1$.

The heat current definitions, Eqs. (7) and (8) are obviously equivalent: They are related based on the assumption of a white Gaussian noise. As we mentioned in the Introduction, the interface definition is appealing in formal calculations: It allows the construction of a closed-form definition for the heat current even in anharmonic models, as long as the system-bath coupling is bilinear. Furthermore, it bypasses the problem of defining a heat current operator for quantum systems, which is non-unique³⁷. The interface expression is also appealing if the conducting system has a complex connectivity with many bonds (say beyond nearest neighbors) contributing to heat propagation. In such a tangled scenario, it seems more feasible to calculate the steady state heat current by measuring the input or output power—between the system and the thermostats. In fact, in experimental

studies the molecular thermal conductance is evaluated in this manner, by measuring the input heat power at the contact region¹⁸. The interface definition is also useful in hybrid models: In a recent study of thermal transport across a metal-polymer interface, heat exchange between the electronic and nuclear degrees of freedom was inferred from the net vibrational heat transfer, from the atoms to the Langevin thermostat, that is, using the interface definition⁴³.

The intramolecular definition is attractive in molecular dynamics simulations: Since in steady state the time-averaged currents $J_M^{(n)}$ are equal for every n , one can perform an additional averaging, $\bar{J}_M \equiv \sum_2^N J_M^{(n)}/(N-1)$, to reduce the error of the individual bond current. This type of averaging can be also implemented in complex networks.

In what follows, we examine the interface and ‘bare’ intramolecular definitions (without site averaging), Eqs. (7) and (8) in classical systems based on numerical simulations for both harmonic and anharmonic junctions as depicted in Fig. 1. We show that it is more challenging to converge J_I to the correct result—compared to J_M . For example, at thermal equilibrium J_M more feasibly approaches the correct behavior (zero current) even when equipartition of energy is not yet accomplished (due to numerical errors). Away from equilibrium, J_I may display a thermal diode effect for harmonic systems, which is a numerical artifact emerging from the finite time step error or the frequency integration error.

III. FREQUENCY DOMAIN: NUMERICAL INTEGRATION

In this Section we focus on harmonic systems and illustrate the flaws of the boundary definition J_I when

working in Fourier’s - frequency space. In the frequency domain, the EOM (4) can be solved as an algebraic problem in steady state, and the different correlation functions (position-position, velocity-position, velocity-velocity) can be obtained analytically.

To simplify notation, in the following derivations we formally include a local thermal bath at each site, therefore introduce the friction coefficients γ_n for every site, $n = 1, 2, \dots, N$. In simulations we set $\gamma_{2,3,\dots,N-1} = 0$ and recover the junction setup with only two heat baths at the boundaries.

A. Discussion of heat current definitions

For harmonic systems, the intramolecular heat current evaluated between sites n and $n+1$ —also referred to as bond current—is given by^{8,44} (masses are set to unit),

$$J_M^{(n+1)} = -k_{n,n+1} \sum_{m=1,N} \gamma_m k_B T_m \int_{-\infty}^{\infty} d\omega \frac{\omega}{\pi} \text{Im} [(G^r(\omega))_{n,m} (G^a(\omega))_{m,n+1}]. \quad (9)$$

Here, $\mathbf{G}^r(\omega)$ is a symmetric matrix, corresponding to the retarded Green’s function⁸. For example, for a 3-site chain with nearest neighbor interaction we write $(k_{i,j} = k_{j,i})$,

$$\mathbf{G}^r(\omega) = \begin{bmatrix} -\omega^2 + k_{2,1} + k_{1,0} - i\gamma_1\omega & -k_{2,1} & 0 \\ -k_{2,1} & -\omega^2 + k_{2,1} + k_{3,2} - i\gamma_2\omega & -k_{3,2} \\ 0 & -k_{3,2} & -\omega^2 + k_{3,2} + k_{4,3} - i\gamma_3\omega \end{bmatrix}^{-1}$$

Furthermore, $G^a = (G^r)^\dagger$ thus $[(G^r(\omega))_{n+1,m}]^* = (G^a(\omega))_{m,n+1}$.

To calculate the interface current, we evaluate the momentum autocorrelation function⁸,

$$\langle p_n^2 \rangle = \frac{1}{\pi} \int_{-\infty}^{\infty} d\omega \omega^2 \sum_m |(G^r(\omega))_{n,m}|^2 \gamma_m k_B T_m. \quad (10)$$

Note that at thermal equilibrium, with all temperatures identical, we reach energy equipartition and we obtain

the normalization condition:

$$N_n \equiv \frac{1}{\pi} \int_{-\infty}^{\infty} d\omega \omega^2 \sum_m |(G^r(\omega))_{n,m}|^2 \gamma_m = 1. \quad (11)$$

In Appendix A we point out that the normalization condition in fact is a strict sum rule condition for the spectral function of the chain. Based on the definition (8),

the interface current at site 1 is given by

$$\begin{aligned}
 J_I^{(1)} &= -\gamma_1 (\langle p_1^2 \rangle - k_B T_1). \\
 &= -\sum_m \frac{\gamma_1 \gamma_m}{\pi} \int_{-\infty}^{\infty} d\omega \omega^2 |(G^r(\omega))_{1,m}|^2 k_B T_m + \gamma_1 k_B T_1.
 \end{aligned}
 \tag{12}$$

We thus have two working definitions for the heat current: (i) The intramolecular current Eq. (9). (ii) The interface definition at site 1, Eq. (12), with an analogous expression at site N .

In simulations, the limits of integrations are truncated at $\pm\omega_c$, and one would naively assume that taking ω_c to be one order of magnitude larger than the thermal energy $k_B T$ and the friction coefficient γ should suffice for achieving converged results. However, as we now show with simulations, the interface definition (12) is challenging to converge to the correct result even when ω_c is made quite high, unlike the intramolecular calculation. This problem manifests itself as a residual J_I current at thermal equilibrium and as an erroneous rectification effect for J_I in harmonic junctions.

B. Simulations

We simulate heat transport with the intramolecular definition $J_M^{(n)}$ using Eq. (9). It can be evaluated anywhere in the chain, and we use the chain's center (results were identical for any n). The interface definition at site 1, $J_I^{(1)}$ is calculated from Eq. (12); an analogous expression is used for the interface current at the other end, $J_I^{(N)}$. In simulations we set $\pm\omega_c$ as the limits of integration. The integration interval $\delta\omega$ was taken small enough; we confirmed that it did not introduce an integration error. Regarding units used: For simplicity in simulations $k_B = 1$, $\hbar = 1$. Therefore, ω_c , γ , T , and $\sqrt{k/m}$ have the same units (energy). The simulated heat current has units of energy squared. If, for example we set the energy unit to 20 meV, we get $T = 1 \rightarrow k_B T = 20$ meV, $\gamma = 0.1 \rightarrow \gamma = 0.5$ ps $^{-1}$, $\sqrt{k/m} = 1 \rightarrow \sqrt{k/m} = 160$ cm $^{-1}$ and the resulting current, $J = 0.2 \rightarrow \sim 20$ nW.

Thermal equilibrium. We test the equilibrium scenario in Fig. 2. While J_M is identically zero irrespective of the value of ω_c , we find that J_I shows a significant error, a nonzero current (compare magnitude to Fig. 3). We further study the mean-square momentum, which should be equal to $k_B T$ at equilibrium based on energy equipartition. The kinetic energy deviates from the equipartition value at the boundaries, and this deviation reduces as we increase ω_c . However, it is notable that $J_M = 0$ irrespective of the accuracy of energy equipartition, while the quality of J_I relies on this property. Essentially, in the intramolecular definition every frequency component

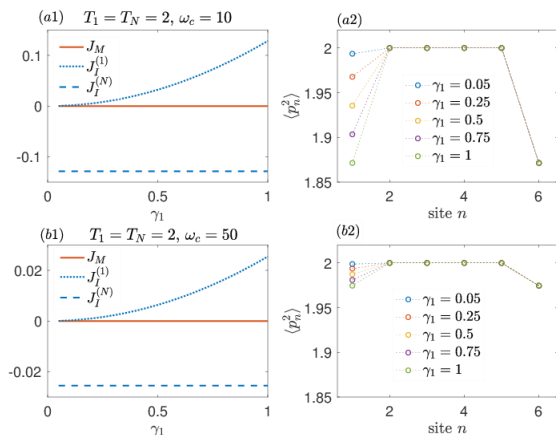


FIG. 2. Frequency domain equilibrium simulations with $T_1 = T_N$. (a1) Heat current and (a2) mean square momentum as a function of γ_1 for $\omega_c = 10$ and (b1)-(b2) $\omega_c = 50$. Here and below the integration step is $\delta\omega = 5 \times 10^{-3}$. The chain includes $N = 6$ sites and we set $\gamma_N = 1$ while varying γ_1 . Other parameters are $k = 1$, $T_1 = T_N = 2$.

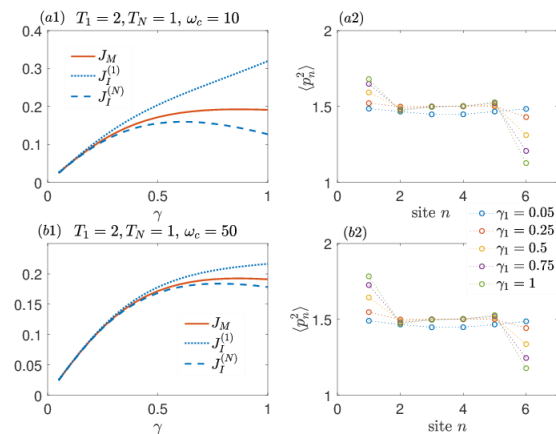


FIG. 3. Steady state heat current under a temperature bias $T_1 = 2$ and $T_N = 1$, frequency domain simulations. (a1) Heat current and (a2) mean-square momentum at $\omega_c = 10$ and (b1)-(b2) $\omega_c = 50$ with the integration step $\delta\omega = 5 \times 10^{-3}$. The chain includes $N = 6$ sites, $k = 1$, and we vary the friction coefficient at the boundaries $\gamma = \gamma_{1,N}$ in a symmetric manner.

in the current is individually cancelled out between the two heat baths. Therefore, even if the upper limit of integration is not high enough to achieve equipartition, the current is identically zero at equilibrium.

While in Figure 2 we use $\gamma_1 \neq \gamma_N$, we emphasize that structural asymmetry is not the source of the problem. When we repeat this simulation with $\gamma_1 = \gamma_N$, we get that $J_I^{(N)}$ becomes a mirror image of $J_I^{(1)}$, with both currents significantly deviating from the correct (zero current) value.

Nonequilibrium steady state. In Fig. 3 we apply a tem-

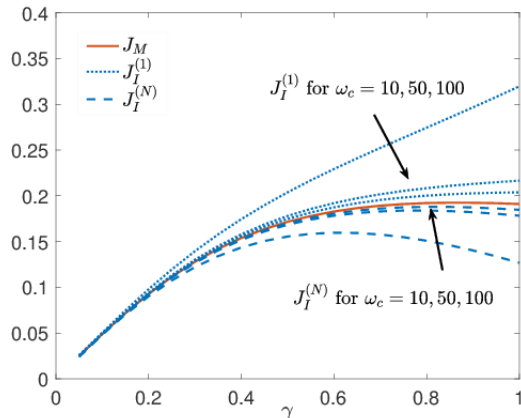


FIG. 4. Convergence of the interface heat current upon increasing ω_c , frequency domain simulations. We use $\gamma = \gamma_{1,N}$, $T_1 = 2$, $T_N = 1$, $N = 6$, $k = 1$. The interface currents $J_I^{(1)}$ (dotted line) and $J_I^{(N)}$ (dashed) approach the intramolecular definition (full) as we increase ω_c . The intramolecular current does not change with ω_c .

perature difference across the junction and compare the cases $\omega_c = 10$ and $\omega_c = 50$. While J_M does not depend on the integration limits at this resolution, and it is well converged (see also Fig. 4), we find that $J_I^{(1)}$ and $J_I^{(N)}$ significantly deviate from the correct answer, showing a strong dependence on ω_c . Furthermore, when we plot the mean squared-momentum (panels a2 and b2) we find that modifying ω_c slightly changes the value at the boundary atoms, 1 and N . It is notable that a 5% modification in $\langle p_1^2 \rangle$ (as we tune ω_c from 10 to 50) translates to about 50% shift in the magnitude of the interface current, illustrating its strong sensitivity to the average energy at the boundaries.

We further demonstrate the slow convergence of J_I with ω_c in Fig. 4. While J_M converges once $\omega_c \approx 10k_B T_a$ (the full line for J_M does not vary as we increase ω_c), $J_I^{(1)}$ and $J_I^{(N)}$ still visibly deviate from the correct answer even for $\omega_c \approx 100k_B T_a$; T_a is the average temperature.

Erroneous thermal rectification. Harmonic junctions connected to two heat baths at different temperatures cannot rectify heat^{45–48}. That is, the magnitude of the heat current should be the same when interchanging the temperatures of the reservoirs, T_1 by T_N . Fig. 5 shows that the rectification ratio is identically one when adopting the intramolecular definition, $R \equiv |J_M(F)/J_M(R)| = 1$. However, the interface current shows a (faulty) significant rectification, up to a factor 2 if the integration is not carried out to large enough ω_c . In panel (b) we repeat the calculation for a larger ω_c . While there is a marked improvement with the interface currents approaching the intramolecular definition, the rectification ratio is still substantial as we present in panel (b2).

C. Error Analysis

What is the reason for the puzzling-faulty behavior of the interface current? In short, the interface current can be converted to the Landauer formula only after using a sum rule, which is difficult to converge. In contrast, the intramolecular current reduces to the Landauer formula based on an identity for the integrands. Let us play with Eq. (12):

$$\begin{aligned}
 & \sum_m \frac{\gamma_1 \gamma_m}{\pi} \int_{-\infty}^{\infty} d\omega \omega^2 |(G^r(\omega))_{1,m}|^2 k_B T_m - \gamma_1 k_B T_1 \\
 &= \sum_m \frac{\gamma_1 \gamma_m}{\pi} \int_{-\infty}^{\infty} d\omega \omega^2 |(G^r(\omega))_{1,m}|^2 k_B (T_m - T_1) \\
 &+ \sum_m \frac{\gamma_1 \gamma_m}{\pi} \int_{-\infty}^{\infty} d\omega \omega^2 |(G^r(\omega))_{1,m}|^2 k_B T_1 - \gamma_1 k_B T_1. \\
 &= \sum_m \frac{\gamma_1 \gamma_m}{\pi} \int_{-\infty}^{\infty} d\omega \omega^2 |(G^r(\omega))_{1,m}|^2 k_B (T_m - T_1).
 \end{aligned} \tag{13}$$

The last step relies on the normalization condition, Eq. (11). With these simple manipulations, we received the multi-terminal Landauer formula for heat transport. If only the first and last sites couple to thermostats, this last expression precisely corresponds to the two-terminal Landauer formula, $J_{Land} = \frac{\gamma_1 \gamma_N}{\pi} \int_{-\infty}^{\infty} d\omega \omega^2 |(G^r(\omega))_{1,N}|^2 k_B (T_1 - T_N)$ ^{45,46,49}.

Obviously, the Landauer formula for heat currents does not suffer from pathologies such as a nonzero current at thermal equilibrium or a manifestation of a diode effect—given its explicit dependence on the temperature difference. We have therefore just proved that J_I of Eq. (12) is mathematically equivalent to the good-old Landauer formula. Why then does Eq. (12) show computational flaws, e.g. a nonzero current at equilibrium? The answer is that in transforming Eq. (12) to the Landauer form we relied on the normalization integral (11). To achieve an accurate normalization, the limits of integration (ω_c) need to be extended to very high frequencies. Specifically, we need to use $\omega_c > 100k_B T$ to get an error smaller than 10%, that is $|J_I^{(1)}/J_I^{(N)}| < 1.1$.

From Eq. (13) we also note that since $\sum_m \frac{\gamma_1 \gamma_m}{\pi} \int_{-\omega_c}^{\omega_c} d\omega \omega^2 |(G^r(\omega))_{1,m}|^2 < \gamma_1$, the interface current at site ‘1’ should exceed the correct value for $T_1 > T_N$ when un-converged, $J_I^{(1)} > J_M$, and the other way for $J_I^{(N)}$.

Complementing this discussion, in Appendix B we prove that the intramolecular current (9) reduces to a Landauer form with an explicit dependence on the temperature difference by utilizing a trivial identity for the integrands—that does not depend on the limits of integrations—thus does not suffer from numerical pathologies.

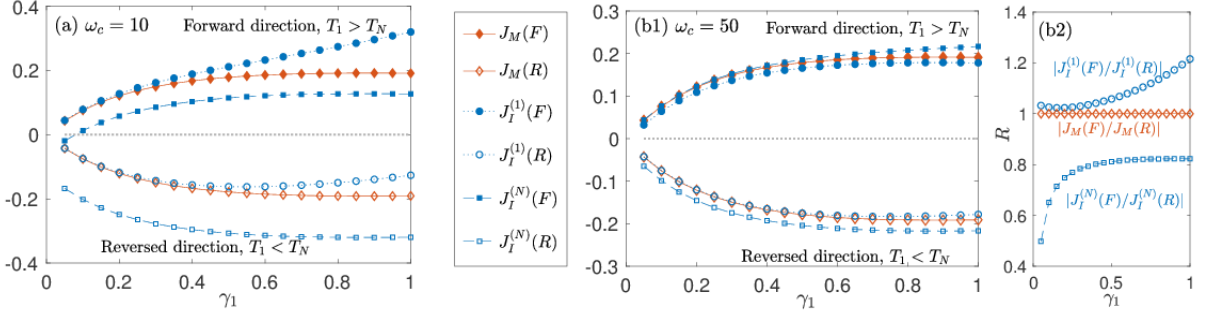


FIG. 5. Erroneous thermal rectification effect for harmonic junctions based on the interface definition using frequency domain simulations. We present the heat currents in the forward (F) and reversed (R) directions for $\omega_c = 10$ (a) and $\omega_c = 50$ (b1). The magnitude of J_I is different in the forward and reversed directions while $|J_M(F)| = |J_M(R)|$. In panel (b2) we display the rectification ratio for the $\omega_c = 50$ case. $R \equiv |J(F)/J(R)|$ is calculated by dividing currents in the forward direction $T_1 > T_N$ (filled symbols) by currents in the reversed direction $T_1 < T_N$ (empty symbols). We use $T_1 = 2$, $T_N = 1$, $N = 6$, $k=1$, $\gamma_N=1$.

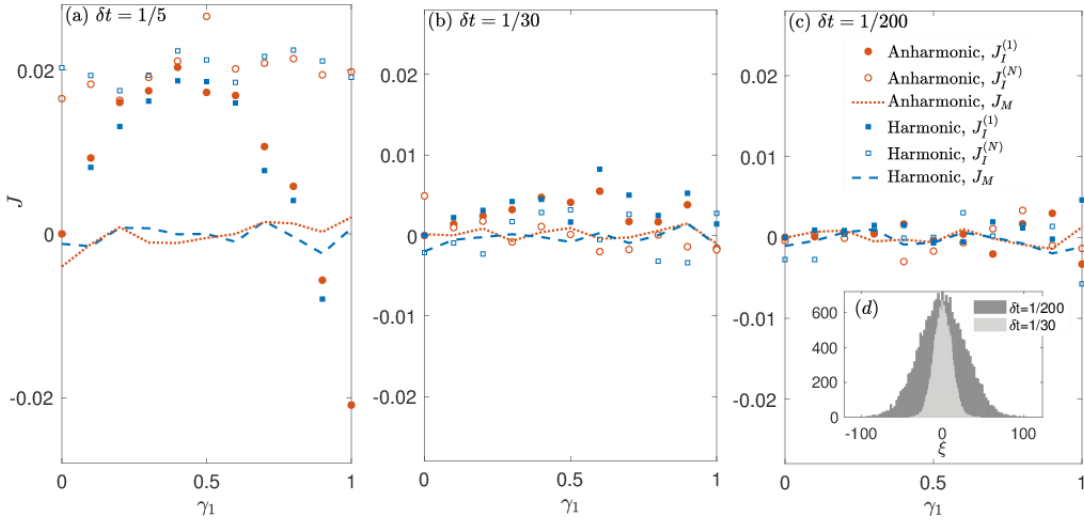


FIG. 6. Molecular dynamics simulations of an equilibrium setup with $T_1 = T_N = 1$. (a)-(c) Heat current as a function of γ_1 for harmonic and anharmonic chains. The intramolecular current is close to zero even for a rough time step, while the interface currents show substantial errors, which can be reduced when taking a smaller time step. Parameters are $N = 6$, $\gamma_N = 1$, $k = 1$, and the integrator is RK4. Unless otherwise mentioned, here and in figures below the time interval is $\tau = 90$ and J_M is calculated between sites 3 and 4. (d) Histograms of the gaussian random noise generated for two different time steps, showing the broadening of the histograms as the time step becomes shorter.

IV. TIME DOMAIN: MOLECULAR DYNAMICS SIMULATIONS

The exact Green's function method described above is limited to harmonic models. While a Meir-Wingreen type expression can be derived for anharmonic systems⁵¹, calculations of the Green's function involved can only be done perturbatively for the anharmonic contributions^{9,10}. In classical systems, molecular dynamics simulations are therefore central for the study of phononic heat conduction.

In this Section we simulate phononic conduction in har-

monic and anharmonic molecular junctions using classical molecular dynamics simulations and testing the performance of the two (intramolecular, interface) definitions. We set the initial conditions, then time-evolve the equations of motion for long enough production time to get a trajectory corresponding to the steady state limit. We numerically integrate the Langevin equation (2) testing three different integrators, the fourth-order Runge-Kutta (RK4) method, the Brünger-Brooks-Karplus (BBK) integrator⁵², and with the method developed by Vanden-Eijnden and Ciccotti⁵³, which we refer to as the VEC integrator.

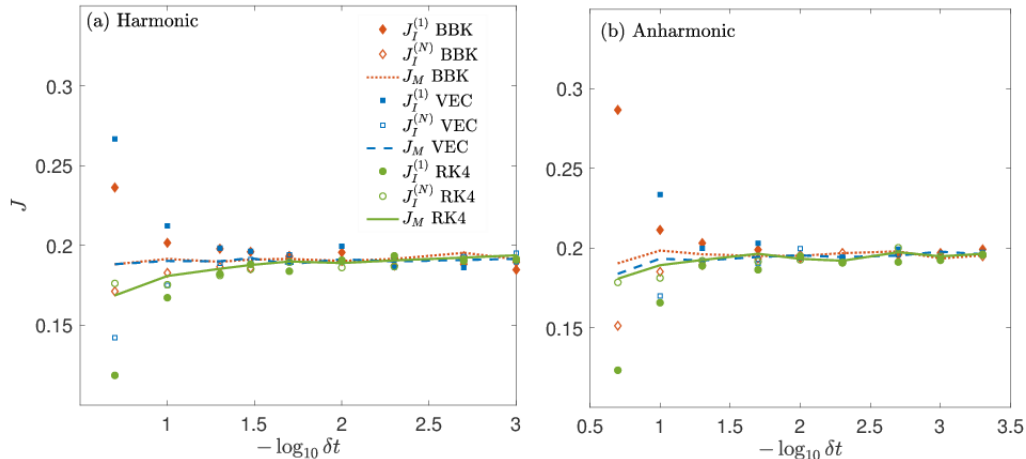


FIG. 7. Molecular dynamics simulations of heat currents in a nonequilibrium steady state for (a) harmonic and (b) anharmonic potentials. We use $T_1 = 2$, $T_N = 1$, $N = 6$, $k = 1$, $\gamma_1 = \gamma_N = 1$ and we test three integrators: RK4, BBK and VEC.

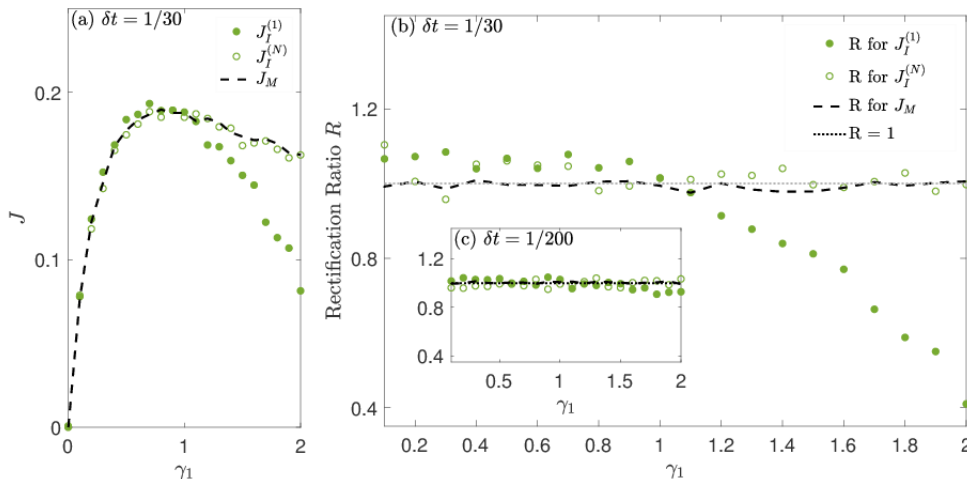


FIG. 8. An erroneous thermal rectification effect in harmonic systems based on molecular dynamics simulations. (a) Current and (b) erroneous rectification using RK4 for $\delta t = 1/30$. (c) Rectification disappears when using a finer time step of $\delta t = 1/200$. We use $N = 6$, $\gamma_N = 1$, $k = 1$, $T_H = 2$ and $T_C = 1$.

To compute heat currents, we wait for the system to reach a steady state, then at each time step (duration δt) within a time interval τ we record the heat currents. To take an average over realizations of the noise we repeat this process over an ensemble of size N_ζ , and we average the $\frac{\tau}{\delta t} \times N_\zeta$ values of currents. We consider both harmonic and anharmonic potentials. In the anharmonic case we use $V(x_1, \dots, x_n) = \frac{1}{4} \sum_{n=2}^N k(x_n - x_{n-1} - a)^4$ for the interparticle potential energy, and the same form for the contact coupling V_B . Unless otherwise specified, we set $k = 1$ in the potential energy, use $\gamma = 0.1 - 2$, and average over an ensemble size $N_\zeta = 4000$ and a time interval $\tau = 90$, while using a simulation time step in the range $\delta t = 10^{-3} - 0.5$.

Our main finding in this section is that, similarly to observations in the frequency domain, the intramolecular heat current is advantageous over the interface currents. The intramolecular current converges faster when decreasing δt than the interface current. While the intramolecular definition correctly shows a vanishing current at equilibrium and the absence of thermal rectification effect for harmonic junctions, for corresponding parameters the interface currents display finite current at equilibrium, and a rectification effect. Overall, we argue that the impact of the propagation time step (δt) error in molecular dynamics simulations is analogous to the role of the frequency cutoff ω_c in the frequency domain.

A. Averaged heat current

Thermal equilibrium. In Figure 6 we study the equilibrium scenario with $T_1 = T_N$ using the RK4 method. We find that the intramolecular current is very close to zero even for a rough time step. In contrast, for the same time step discretization, the interface expressions at the left and right sides display significant erroneous heat currents.

We make the following observations: (i) The erroneous interface current is suppressed when reducing the time step from $\delta t = 0.2$ to $\delta t = 0.03$. This improvement is not due to the additional averaging associated with increasing the trajectory time, $\tau/\delta t$ for a shorter time step. Indeed we verified that keeping δt fixed while increasing τ does not suppress the flawed current J_I . (ii) The interface definition inadequately performs (for large δt) in both harmonic and anharmonic systems. (iii) In some cases, a symmetrization of the interface current may assist to reduce its error, yet it does not cancel the error exactly. (iv) As we continue and reduce the time step from $\delta t = 1/30$ to $\delta t = 1/200$, we do not observe additional improvements in the behavior of the heat current, demonstrating that this residual error is associated with the ensemble average. We note that as we reduce the time step, more intense random forces are taken into account, see the histogram of the gaussian noise in panel (d) of Fig. 6. We performed additional simulations for other chain lengths, $N = 4 - 10$ and confirmed that our observations were unchanged. Generally, it was more difficult to converge the interface current with increasing chain length.

Steady state heat current. In Fig. 7 we study the currents in harmonic and anharmonic cases under a temperature bias. First we confirm that the harmonic intramolecular current agrees with calculations done in the frequency domain, see Fig. 3. We find that the error of the interface currents drops when reducing the time step. Note that since the coefficient k in the potential energy has a different physical dimension for harmonic and anharmonic junctions, we cannot meaningfully compare these results. A relevant comparison could be made by studying a model with harmonic plus anharmonic terms, slowly turning on the anharmonicity.

We test three different integrators and conclude that independently of the integrator, the intramolecular current definition is advantageous over the interface current, as the latter requires more computational effort (shorter time step) to converge to the correct result. It is intriguing to note that in the BBK and VEC methods $J_I^{(1)} > J_M$, while the opposite holds for RK4. To explain these trends one needs to carefully study errors associated with the different integrators, and how these errors impact energy equipartition.

Thermal rectification. We test the (faulty) development of the thermal rectification effect in harmonic junctions in Fig. 8. First, in panel (a) we display the heat current as a function of γ_1 . These simulations were per-

formed in the “forward” direction, with $T_1 > T_N$. Next, in panels (b)-(c), we analyze the rectification ratio R . While the intramolecular current shows no rectification, the interface current $J_I^{(1)}$ displays the effect, and it can be substantial for large asymmetry. We repeated these simulations while fixing γ_1 and varying γ_N . In this case, large rectification shows at the other contact current, $J_I^{(N)}$. In Ref.⁴² it was argued, based on molecular dynamics simulations, that a linearized (harmonic) model could support the thermal diode effect. We point that this observation may result from the pathologies of the interface current (employed in that study), when improperly converged.

B. Heat exchange fluctuation relation

Beyond the averaged current, we are interested in the full probably distribution function of heat exchange. This would allow us to confirm that the simulation protocol is correct—satisfying the steady state exchange fluctuation symmetry, $P(Q)/P(-Q) = e^{\Delta\beta Q}$ ⁵⁴. Here, Q the integrated heat current within a certain duration, $P(Q)$ is the probability distribution function of heat exchange Q , and $\Delta\beta = 1/T_C - 1/T_H$, T_C (T_H) is the temperature of the cold (hot) thermal bath.

To produce a histogram of the heat exchange, we follow many trajectories of duration τ and calculate the integrated currents $Q(\tau) \equiv \int_{\tau_0}^{\tau_0+\tau} J(t)dt$. The time τ_0 is taken long enough so as initial conditions become irrelevant. We calculate the integrated currents using the intramolecular and interface definitions, and construct the three histograms.

First, we point out that to calculate the integrated interface current, $Q_I(\tau)$, we cannot use Eq. (8), since this expression already relies on performing the average $\langle \xi_n(t)p_n(t) \rangle$. Indeed, based on the definition $J_I^{(1)} = -\gamma_1 (\langle p_1(t)^2 \rangle / m_1 - k_B T_1)$, the stochastic current $J_I^{(1)}$ cannot be larger than $\gamma_1 k_B T_1$. Similarly, the stochastic current at the other end, $J_I^{(N)}$ cannot take values below $-\gamma_N k_B T_N$. To properly generate $P(Q_I)$ we therefore resort to the original definition of the interface current, e.g. $J_I^{(N)} = \frac{\gamma_N}{m_N} \langle p_N(t)^2 \rangle - \frac{1}{m_N} \langle \xi_N(t)p_N(t) \rangle$. However, in simulations we encounter an additional challenge in calculating $\langle \xi_n(t)p_n \rangle$, which we now explain. Recall that in sophisticated integrators one generates the value at $t + \delta t$ based on intermediate calculations, between t and $t + \delta t$. For example, in the BBK scheme we first calculate the momentum at the half interval, $t + \delta t/2$ (the update is more complex in the RK4 method). As such, it becomes unclear whether in the average $\langle \xi_n(t)p_n \rangle$ one should take the momentum at the midpoint $t + \delta t/2$, or after a full time step $t + \delta t$. From simulations we noted that this average delicately depends on this choice; in both RK4 and the BBK methods, we found that to produce the correct average, $\langle \xi_n(t)p_n \rangle = \gamma m_n k_B T_n$, the momentum had to be selected at the midpoint, $t + \delta t/2$.

In Fig. 9, we present histograms of heat exchange us-

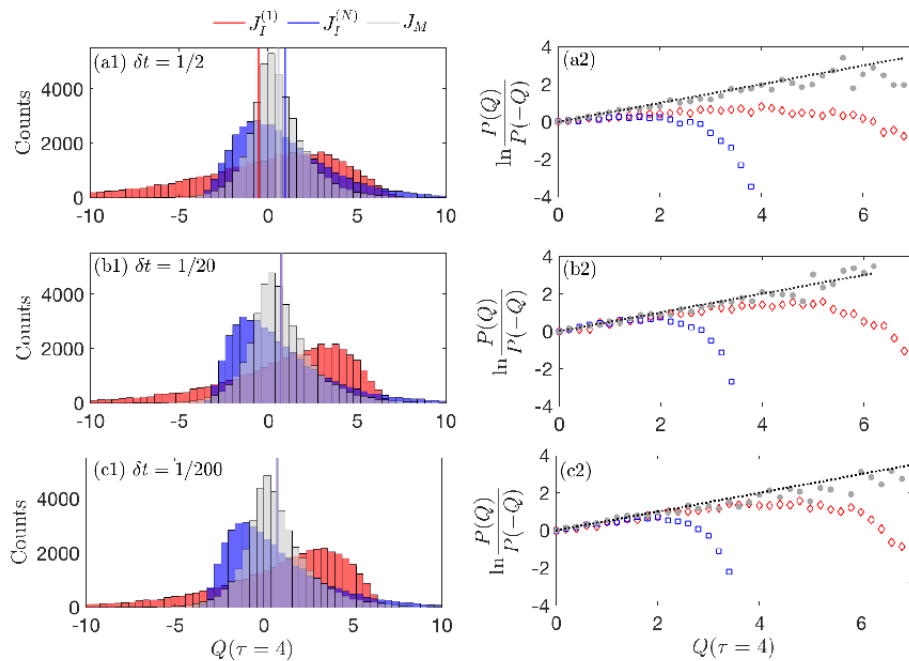


FIG. 9. (a1)-(c1) Probability distributions of observed integrated heat currents $P(Q)$ within a duration τ using the RK4 integrator. Reducing δt does not much alter the shape of the distribution, but it causes the means (vertical lines) to converge. The interactions in the chain are harmonic with and we adopt $k = 1$, $\gamma_{1,N} = 1$, $N = 4$, $T_1 = 2$ and $T_N = 1$. In panels (a2)-(c2) we test the fluctuation symmetry. It approaches the correct slope (dotted) for the intramolecular current, $\Delta\beta = 1/T_C - 1/T_H = 1/2$, while for the interface currents deviations show up even as the averaged current converges to the correct value.

ing three different time steps. We further test the fluctuation symmetry at the right panels. We find that the intramolecular current obeys the fluctuation symmetry, $P(Q)/P(-Q) = e^{\Delta\beta Q}$ even with a rough time step. In contrast, the interface currents violate this symmetry, *even when the averaged currents are converged once the time step is short enough in panels (b) and (c)*. We conclude that in molecular dynamics simulations, the interface definition should not be used to study the full counting statistics: (i) Its construction is ill-defined (as mentioned above, we used momentum at the half step to enforce the correct average). (ii) The shape of the distribution is incorrect even when the mean converges to the correct steady state value.

C. Comparison between integrators

Results presented in Figs. 6, 8 and 9 were obtained using the RK4 integrator. In Appendix C we include additional demonstrations using the BBK integrator⁵². The three integrators show that the intramolecular current definition is advantageous over the interface current: the latter requires more computational effort (shorter time step) to converge to the correct result, and its distribution violates the fluctuation symmetry. We recall that the two definitions of the current involve different correlation functions (position-velocity in the intramolecular

and velocity-squared at the boundaries). While previous studies compared the performance of different integrators against each other, see e.g. Ref.⁵⁵, our analysis here concerns the convergence of different correlation functions with a given integrator. It is interesting to note that the RK4, while not specifically designed to propagate a stochastic differential equation, converges the intramolecular current very well. We further note that the Runge-Kutta integrator is commonly used in fundamental physics studies of anomalous heat transport in one-dimensional systems; some prominent studies include⁵⁶⁻⁵⁸. In contrast, the BBK and the VEC integrators are popular in molecular dynamics simulations of biomolecules and materials.

V. SUMMARY

We focused on the problem of phononic heat transport in nanojunctions and asked an elementary question: Which definition for the heat current best performs in simulations? We argued that while the interface definition is advantageous in formal derivations and in the quantum domain, in classical simulations one should employ the intramolecular definition as it shows a superior convergence.

Considering harmonic junctions, we simulated heat current in the frequency and time domains. Frequency-

domain calculations were done in the language of Green's functions. We showed that the interface definition was poorly converged when truncating high frequency modes, since it relied on a sum rule to converge. In contrast, by construction, the intramolecular current showed favorable properties: The heat current was identically zero at equilibrium and a diode effect was disallowed.

In the time domain, we performed corresponding molecular dynamics simulations and demonstrated that the interface definition required a finer time step to converge, compared to the intramolecular expression. The deficiencies of the interface current manifested themselves in an unphysical behavior of the heat current at equilibrium, with a difficulty to achieve equipartition of energy close to the interface, and in the development of a diode effect for harmonic junctions. These issues were observed with different integrators, RK4, BBK and the VEC. Insights on the poor performance of the interface currents could be achieved based on the upside/downside statistical analysis suggested in Refs^{59,60}. While so far much effort had been placed on comparing the performance of different integrators, here we emphasize that using different working definitions for an observable may result in different convergence behavior.

Given significant advancements in experimental studies of vibrational heat transport across single molecules, and similarly, progress in emulating transport problems with engineered chains such as trapped ions structures^{61,62}, it becomes increasingly important to perform accurate numerical simulations so as to bring useful predictions and gather fundamental understandings of mechanisms. Furthermore, to probe noise-precision trade off relations in thermal machines, we need to simulate both the current and its fluctuations in a nonequilibrium steady state⁶³⁻⁶⁵. As we showed here, the intramolecular definition had correctly captured the fluctuations of heat exchange by delivering the steady-state fluctuation symmetry, therefore it acted as a benchmark. In contrast, the interface definition of heat exchange showed violations of the fluctuation symmetry. Even when the averaged current converged to the correct result, fluctuations were not correctly described by the interface expression.

In principle, one could always reduce the time step in molecular dynamics simulations and simply verify convergence, irrespective of the definition employed. Our message is that: (i) Before convergence is reached, the interface definition leads to incorrect physical predictions, unlike the intramolecular current. (ii) The interface definition cannot properly generate the full counting statistics of heat exchange. It would be interesting to go beyond a delta-impulsive noise process and perform similar analysis for non-Markovian thermostats^{66,67}.

ACKNOWLEDGMENTS

DS acknowledges the NSERC discovery grant and the Canada Chair Program. BKA gratefully acknowledges

the start-up funding from IISER Pune and the hospitality of the Department of Chemistry at the University of Toronto. The authors acknowledge illuminating discussions with Junjie Liu.

Data Availability. The data that support the findings of this study are available from the corresponding author upon reasonable request.

APPENDIX A: THE NORMALIZATION CONDITION AS A SUM RULE

In this Appendix we show that the normalization condition Eq. (11) is in fact a strict sum rule condition for harmonic oscillator systems given by the Hamiltonian Eq. (1), with the beads further coupled to independent heat baths. This is true for quantum and classical systems. For generality, we present the argument in a quantum mechanical description, treating position and momentum as operators. We first write down the standard definitions for the retarded and advanced Green's functions,

$$\begin{aligned} G_{ij}^r(t) &= -\frac{i}{\hbar}\theta(t)\langle [x_i(t), x_j(0)] \rangle, \\ G_{ij}^a(t) &= \frac{i}{\hbar}\theta(t)\langle [x_i(t), x_j(0)] \rangle, \end{aligned} \quad (\text{A1})$$

where the operators are written in the Heisenberg picture. We further assume that the Green's functions are time-translational invariant and therefore depend only on one time argument. Upon taking the first derivative with respect to time for the Green's functions, one can simply receive the following relation

$$\dot{G}_{ij}^r(t) - \dot{G}_{ij}^a(t) = -\frac{i}{\hbar}\langle [p_i(t), x_j(0)] \rangle, \quad (\text{A2})$$

which for time $t = 0$, leads to an interesting observation

$$\dot{G}_{ij}^r(t=0) - \dot{G}_{ij}^a(t=0) = -\frac{i}{\hbar}\langle [p_i(0), x_j(0)] \rangle = -\delta_{ij}. \quad (\text{A3})$$

In matrix notation, this relation implies,

$$\dot{\mathbf{G}}^r(t=0) - \dot{\mathbf{G}}^a(t=0) = \mathbf{I}. \quad (\text{A4})$$

In frequency domain, after performing the Fourier transformation, the above relation translates to

$$\int_{-\infty}^{\infty} \frac{d\omega}{2\pi} \omega \mathbf{A}(\omega) = \mathbf{I}, \quad (\text{A5})$$

where $\mathbf{A}(\omega) = i[\mathbf{G}^r(\omega) - \mathbf{G}^a(\omega)]$ is known as the spectral matrix. Note that this particular sum-rule is valid for arbitrary oscillator system. For harmonic junctions coupled to independent baths, one can further get a closed expression for the spectral matrix, given by

$$\mathbf{A}(\omega) = 2\omega \mathbf{G}^r(\omega) \mathbf{\Gamma}(\omega) \mathbf{G}^a(\omega), \quad (\text{A6})$$

where $\Gamma(\omega)$ is a $N \times N$ diagonal matrix with entries γ_n . The diagonal components of Eq. (A5) along with the above relation gives the sum rule in Eq. (11).

APPENDIX B: PROPERTIES OF THE INTRAMOLECULAR DEFINITION FOR HARMONIC SYSTEMS

A. Derivation of the intramolecular current

The intramolecular heat current in harmonic chains, evaluated between sites n and $n + 1$ is given by^{8,44,68}

$$J_M^{(n+1)} = -k_{n,n+1} \sum_m \gamma_m k_B T_m \int_{-\infty}^{\infty} d\omega \frac{\omega}{\pi} \text{Im} [G_{n,m}^r(\omega) G_{m,n+1}^a(\omega)]. \quad (\text{B1})$$

Here, $G^a = (G^r)^\dagger$ thus $[G_{n+1,m}^r(\omega)]^* = G_{m,n+1}^a(\omega)$. First, we derive Eq. (B1) from the symmetrized Eq. (7),

$$J_M^{(n+1)} = \frac{k_{n,n+1}}{2} (\langle x_n \dot{x}_{n+1} \rangle + \langle \dot{x}_{n+1} x_n \rangle) = k_{n,n+1} \text{Re}[\langle x_n \dot{x}_{n+1} \rangle]. \quad (\text{B2})$$

We define the greater Green's function as

$$G_{l,m}^>(t,t') = \frac{-i}{\hbar} \langle x_l(t) x_m(t') \rangle, \quad (\text{B3})$$

and as such,

$$\langle x_l(t) \dot{x}_{l+1}(t) \rangle = i\hbar \frac{\partial}{\partial t'} G_{l,l+1}^>(t,t')|_{t' \rightarrow t}. \quad (\text{B4})$$

So far, averages correspond to expectation values over the initial state (since we work in the Heisenberg representation). We now perform a time average, so as to reach the steady state (ss) limit,

$$\langle x_l \dot{x}_{l+1} \rangle_{ss} = i\hbar \int_{-\infty}^{\infty} \frac{d\omega}{2\pi} (i\omega) G_{l,l+1}^>(\omega). \quad (\text{B5})$$

Substituting this relation into Eq. (B2) we get

$$J_M^{(n+1)} = -\hbar k_{n,n+1} \int_{-\infty}^{\infty} \frac{d\omega}{2\pi} \omega \text{Re}[G_{n,n+1}^>(\omega)]. \quad (\text{B6})$$

For harmonic systems in the ohmic bath limit and at high temperature⁸

$$G_{n,n+1}^>(\omega) = \sum_m (-i) \frac{k_B T_m}{\hbar \omega} 2\omega \gamma_m G_{n,m}^r(\omega) G_{m,n+1}^a(\omega). \quad (\text{B7})$$

We substitute this into Eq. (B6) and retrieve the intramolecular current (B1).

B. Proof that the intramolecular current is proportional to the temperature difference

We note that at equilibrium, Eq. (B1) reduces to

$$\sum_m \gamma_m \int_{-\infty}^{\infty} d\omega \frac{\omega}{\pi} \text{Im} [G_{n,m}^r(\omega) G_{m,n+1}^a(\omega)] = 0 \quad (\text{B8})$$

We will discuss this identity in more details starting in Eq. (B12).

We now show that the intramolecular current is proportional to the temperature difference ($T_1 - T_N$), thus (i) it is identically zero at equilibrium, and (ii) it cannot produce a diode effect. Since in our system only γ_1 and γ_N are nonzero, Eq. (B1) becomes

$$J_M^{(n+1)} = -\gamma_1 k_B T_1 k_{n,n+1} \int_{-\infty}^{\infty} d\omega \frac{\omega}{\pi} \text{Im} [G_{n,1}^r(\omega) G_{1,n+1}^a(\omega)] - \gamma_N k_B T_N k_{n,n+1} \int_{-\infty}^{\infty} d\omega \frac{\omega}{\pi} \text{Im} [G_{n,N}^r(\omega) G_{N,n+1}^a(\omega)], \quad (\text{B9})$$

which can be written as

$$J_M^{(n+1)} = -\gamma_1 k_B T_1 k_{n,n+1} \int_{-\infty}^{\infty} d\omega \frac{\omega}{\pi} \text{Im} [G_{n,1}^r(\omega) G_{1,n+1}^a(\omega)] - \gamma_N k_B T_N k_{n,n+1} \int_{-\infty}^{\infty} d\omega \frac{\omega}{\pi} \text{Im} [G_{n,N}^r(\omega) G_{N,n+1}^a(\omega)] - \gamma_1 k_B T_N k_{n,n+1} \int_{-\infty}^{\infty} d\omega \frac{\omega}{\pi} \text{Im} [G_{n,1}^r(\omega) G_{1,n+1}^a(\omega)] + \gamma_1 k_B T_N k_{n,n+1} \int_{-\infty}^{\infty} d\omega \frac{\omega}{\pi} \text{Im} [G_{n,1}^r(\omega) G_{1,n+1}^a(\omega)]. \quad (\text{B10})$$

However, based on the equilibrium identity (B8), lines 2 and 3 cancel out, and we get

$$J_M^{(n+1)} = \gamma_1 k_B (T_N - T_1) k_{n,n+1} \int_{-\infty}^{\infty} d\omega \frac{\omega}{\pi} \text{Im} [G_{n,1}^r(\omega) G_{1,n+1}^a(\omega)]. \quad (\text{B11})$$

In this form, we immediately confirm that the heat current vanishes at equilibrium and that it cannot support a diode effect.

C. Analysis of the identity (B8)

Here we prove that the integral condition (B8) is identically zero for any cutoff frequency and that it does not

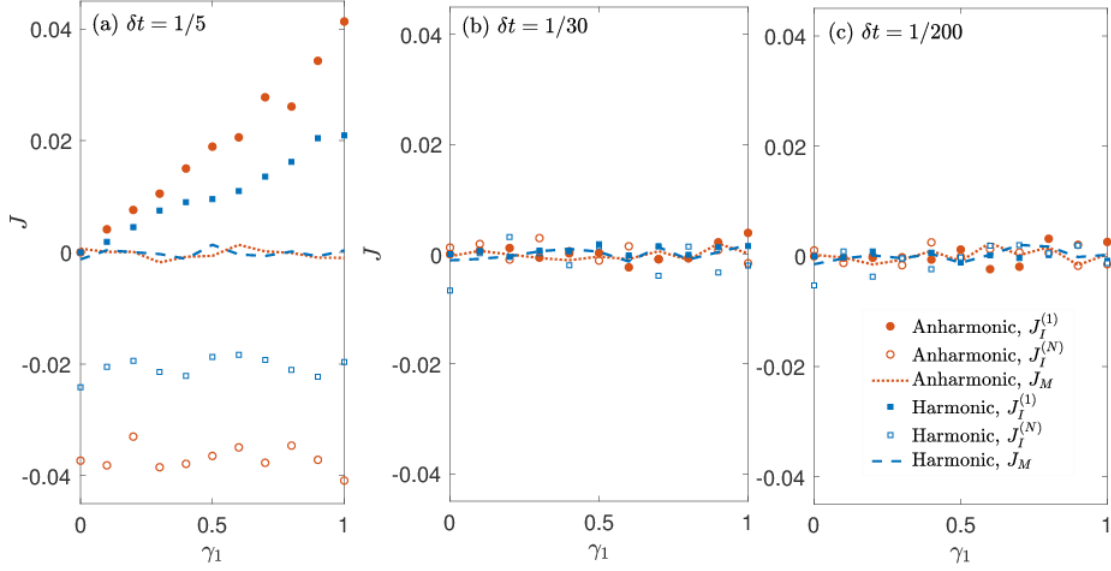


FIG. 10. Molecular dynamics simulations with the BBK scheme of an equilibrium setup with $T_1 = T_N = 1$. (a)-(c) Residual heat current as a function of γ_1 for harmonic and anharmonic chains with different time steps. Parameters are $N = 6$, $\gamma_N = 1$, $k = 1$.

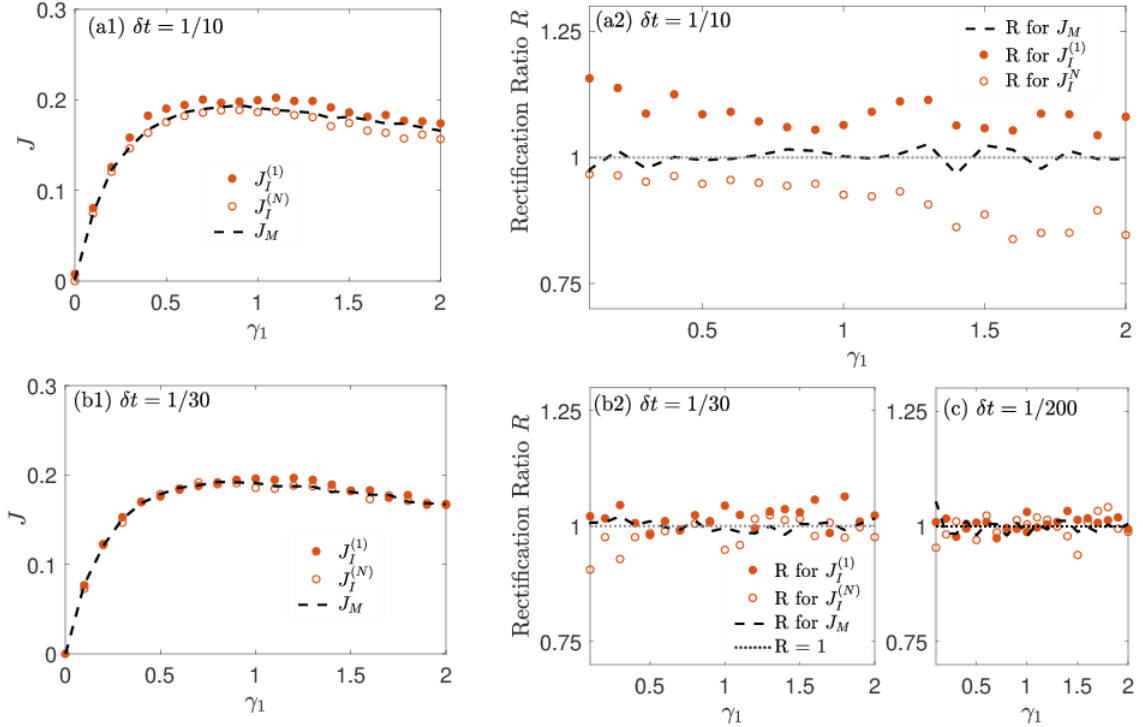


FIG. 11. Molecular dynamics simulations with a BBK scheme demonstrating the erroneous thermal rectification effect in harmonic systems for large δt . (a1) Current and (a2) the incorrect thermal diode effect for $\delta t = 0.1$. (b1)-(b2) As we reduce the time step to $\delta t = 1/30$, the interface current approaches J_M , and the incorrect diode effect is suppressed. (c) Even for very short time step, $\delta t = 1/200$, the intramolecular definition outperforms the interface definition, with a smaller error for R . We use $N = 6$, $\gamma_N = 1$, $k = 1$, $T_H = 2$ and $T_C = 1$.

suffer from numerical convergence problems. This is because the integral vanishes already as a sum of two integrands. We focus on the following relation,

$$\sum_m \gamma_m \int_{-\infty}^{\infty} d\omega \frac{\omega}{\pi} \text{Im} [G_{n,m}^r(\omega) G_{m,n+1}^a(\omega)] = 0. \quad (\text{B12})$$

Since only γ_1 and γ_N are nonzero, it amounts to

$$\begin{aligned} & \gamma_1 \int_{-\infty}^{\infty} d\omega \frac{\omega}{\pi} \text{Im} [G_{n,1}^r(\omega) G_{1,n+1}^a(\omega)] \\ & + \gamma_N \int_{-\infty}^{\infty} d\omega \frac{\omega}{\pi} \text{Im} [G_{n,N}^r(\omega) G_{N,n+1}^a(\omega)] = 0. \end{aligned} \quad (\text{B13})$$

Identifying the spectral function,

$$\begin{aligned} \mathbf{A}(\omega) & \equiv i[\mathbf{G}^r(\omega) - \mathbf{G}^a(\omega)] \\ & = 2\omega \mathbf{G}^r(\omega) \mathbf{\Gamma}(\omega) \mathbf{G}^a(\omega), \end{aligned} \quad (\text{B14})$$

where $\mathbf{\Gamma}(\omega)$ is a diagonal matrix with γ_n on the diagonal, we note that $A_{l,l+1}(\omega) = \sum_m 2\omega \gamma_m G_{l,m}^r(\omega) G_{m,l+1}^a(\omega)$.

However, all the elements of $\mathbf{A}(\omega)$ are real:

$$\begin{aligned} A_{n,m} & = i[G_{n,m}^r(\omega) - G_{n,m}^a(\omega)] \\ & = i[G_{n,m}^r(\omega) - G_{n,m}^{r*}(\omega)] \\ & = -2\Im[G_{n,m}^r(\omega)], \end{aligned} \quad (\text{B15})$$

therefore $\text{Im}[A_{l,l+1}(\omega)] = 0$.

In other words, the two terms in (B13) cancel out for every frequency component, $\gamma_1 \text{Im}[G_{n,1}^r(\omega) G_{1,n+1}^a(\omega)] = -\gamma_N \text{Im}[G_{n,N}^r(\omega) G_{N,n+1}^a(\omega)]$. The intramolecular current thus reduces to a Landauer form based on an identity that holds at the level of the integrand. This is to be contrasted with the interface current that reduces to a Landauer form only after utilizing the sum-rule (11), which is satisfied at the level of the integral.

APPENDIX C: MOLECULAR DYNAMICS SIMULATIONS WITH OTHER INTEGRATORS

The BBK method is one of the most popular integrator in molecular dynamics simulations⁵². In Figs. 10-11 we display simulations that are analogous to Fig. 6 and Fig. 8, respectively, from the main text, but generated here with the BBK integrator, rather than with RK4. First, in Fig. 10 we study the equilibrium case. The intramolecular current is very close to zero, while the interface currents show more substantial deviations. Fig. 11 demonstrates the unphysical thermal diode effect that shows up with the interface definition when not properly converged.

* dvira.segal@utoronto.ca

¹ E. Fermi, J. Pasta, and S. Ulam, Studies of nonlinear problems, Los Alamos Scientific Laboratory report LA-1940 (1955).

² T. Dauxois, Fermi, Pasta, Ulam, and a mysterious lady, *Physics Today* **61**, 55 (2008).

³ D. M. Leitner, Quantum ergodicity and energy flow in molecules, *Advances in Physics* **64**, 445 (2015).

⁴ E. Pop, Energy dissipation and transport in nanoscale devices, *Nano Res.* **3**, 147 (2010).

⁵ N. Li, J. Ren, L. Wang, G. Zhang, P. Hänggi, and B. Li, Colloquium: Phononics: Manipulating heat flow with electronic analogs and beyond, *Rev. Mod. Phys.* **84**, 1045 (2012).

⁶ D. G. Cahill, P. V. Braun, G. Chen, D. R. Clarke, S. Fan, *et al.* Nanoscale thermal transport. II. 2003-2012. *Appl. Phys. Rev.* **1**, 011305 (2014).

⁷ K. Wang, E. Meyhofer, and P. Reddy, Thermal and thermoelectric properties of molecular junctions, *Adv. Func. Mater.* **30**, 1904534 (2020).

⁸ A. Dhar, Heat transport in low dimensional systems, *Adv. Phys.* **57**, 457 (2008).

⁹ J. S. Wang, B. K. Agarwalla, H. Li, and J. Thingna, Nonequilibrium Greens function method for quantum thermal transport, *Frontiers of Physics* **9**, 673 (2014).

¹⁰ D. Segal and B. K. Agarwalla, Vibrational heat transport in molecular junctions, *Ann. Rev. Phys. Chem.* **67**, 185 (2020).

¹¹ Z. Rieder, J. L. Lebowitz, and E. Lieb, Properties of a harmonic crystal in a stationary nonequilibrium state, *J. Math. Phys.* **8**, 1073 (1967).

¹² S. Lepri, R. Livi, and A. Politi, Heat conduction in chains of nonlinear oscillators *Phys. Rev. Lett.* **78**, 1896 (1997).

¹³ R. Livi, Heat transport in one dimension, *J. Stat. Mech.* 034001 (2020).

¹⁴ M. D. Losego, M. E. Grady, N. R. Sottos, D. G. Cahill, and P. V. Braun, Effects of chemical bonding on heat transport across interfaces, *Nat. Mater.* **11**, 502 (2012).

¹⁵ T. Meier, F. Menges, P. Nirmalraj, H. Hölscher, H. Riel, B. Gotsmann, Length-dependent thermal transport along molecular chains, *Phys. Rev. Lett.* **113**, 060801 (2014).

¹⁶ S. Majumdar, J. A. Sierra-Suarez, S. N. Schiffres, W.-L. Ong, C. F. Higgs, A. J. H. McGaughey, and J. A. Malen, Vibrational mismatch of metal leads controls thermal conductance of self-assembled monolayer junctions, *Nano Lett.* **15**, 2985 (2015).

¹⁷ N. Mosso, H. Sadeghi, A. Gemma, S. Sangtarash, U. Drechsler, C. Lambert, and B. Gotsmann, Thermal transport through single-molecule junctions, *Nano Lett.* **19**, 7614 (2019).

- ¹⁸ L. Cui, S. Hur, Z. A. Akbar, J. C. Klöckner, W. Jeong, F. Pauly, S. Y. Jang, P. Reddy, and E. Meyhofer, Thermal conductance of single-molecule junctions, *Nature* **572**, 628 (2019).
- ¹⁹ I. V. Rubtsov and A. L. Burin, Ballistic and diffusive vibrational energy transport in molecules, *J. Chem. Phys. Perspective* **150**, 020901 (2018).
- ²⁰ S. Lepri, R. Livi, and A. Politi, Thermal conduction in classical low-dimensional lattices, *Physics Reports*, **377**, 1 (2003).
- ²¹ H. Datt Pandey and D. M. Leitner, Thermalization and thermal transport in molecules, *J. Phys. Chem. Lett.* **7**, 5062 (2016).
- ²² D. Leitner, Molecules and the eigenstate thermalization hypothesis, *Entropy* **20**, 673 (2018).
- ²³ C.-C. Chien, S. Kouachi, K. A. Velizhanin, Y. Dubi, and M. Zwolak, Thermal transport in dimerized harmonic lattices: Exact solution, crossover behavior, and extended reservoirs, *Phys. Rev. E* **95**, 012137 (2017).
- ²⁴ L. Wang, S. Liu, and B. Li, Validity of local thermal equilibrium in anomalous heat diffusion, *New J. Phys.* **21**, 083019 (2019).
- ²⁵ A. Amir, Y. Oreg, and Y. Imry, Thermal conductivity in 1d: Disorder-induced transition from anomalous to normal scaling, *Europhys. Lett.* **124**, 16001 (2018).
- ²⁶ B. Ash, A. Amir, Y. Bar-Sinai, Y. Oreg, and Y. Imry, Thermal conductance of one dimensional disordered harmonic chains, *Phys. Rev. B* **101**, 121403(R) (2020).
- ²⁷ G. Dematteis, L. Rondoni, D. Proment, F. De Vita, and M. Onorato, Coexistence of Ballistic and Fourier Regimes in the β Fermi-Pasta-Ulam-Tsingou Lattice, *Phys. Rev. Lett.* **125**, 024101 (2020).
- ²⁸ I. Sharony, R. Chen, and A. Nitzan, Stochastic simulation of nonequilibrium heat conduction in extended molecule junctions, arXiv:1908.08617.
- ²⁹ R. Chen, I. Sharony, and A. Nitzan, Local atomic heat currents and classical interference in single-molecule heat conduction, *J. Phys. Chem. Lett.* **11**, 4261 (2020).
- ³⁰ R. Moghaddasi Fereidani and D. Segal, Phononic heat transport in molecular junctions: Quantum effects and vibrational mismatch, *J. Chem. Phys.* **150**, 024105 (2019).
- ³¹ J. C. Klöckner, M. Brkle, J. C. Cuevas, and F. Pauly, Length dependence of the thermal conductance of alkane-based single-molecule junctions: An ab initio study, *Phys. Rev. B* **94**, 205425 (2016).
- ³² Q. Li, M. Strange, I. Duchemin, D. Donadio, and G. C. Solomon, A strategy to suppress phonon transport in molecular junctions using π -stacked systems. *J. Phys. Chem. C* **121**, 7175 (2017).
- ³³ M. Famili, I. Grace, H. Sadeghi, and C. J. Lambert. Suppression of phonon transport in molecular Christmas trees. *Chem. Phys. Chem.* **18**, 1234 (2017).
- ³⁴ D. Martínez Gutierrez, A. Di Pierro, A. Pecchia, L. Medrano Sandonas, R. Gutierrez, M. Bernal, B. Mortazavi, G. Cuniberti, G. Saracco, and A. Fina, Thermal bridging of graphene nanosheets via covalent molecular junctions: A non-equilibrium Greens functions-density functional tight-binding study, *Nano Research* **12**, 791 (2019).
- ³⁵ L. M. Sandonas, A. R. Mendez, R. Gutierrez, J. M. Ugalde, V. Mujica, and G. Cuniberti, Selective transmission of phonons in molecular junctions with nanoscopic thermal baths, *J. Phys. Chem. C* **123**, 9680 (2019).
- ³⁶ B. K. Agarwalla, B. Li, and J. S. Wang, Full-counting statistics of heat transport in harmonic junctions: Transient, steady states, and fluctuation theorems, *Phys. Rev. E* **85**, 051142 (2012).
- ³⁷ L.-A. Wu and D. Segal, Energy flux operator, current conservation and the formal Fourier's law, *J. Phys. A: Math. and Theo.* **42**, 025302 (2009).
- ³⁸ A. Kato and Y. Tanimura, Quantum heat current under non-perturbative and non-Markovian conditions: Applications to heat machines, *J. Chem. Phys.* **145**, 224105 (2016).
- ³⁹ H. M. Friedman, B. K. Agarwalla, and D. Segal, Quantum energy exchange and refrigeration: A full-counting statistics approach, *New J. Phys.* **20**, 083026 (2018).
- ⁴⁰ C. Mejia-Monasterio, A. Politi, and L. Rondoni, Heat flux in one-dimensional systems, *Phys. Rev. E* **100**, 032139 (2019).
- ⁴¹ Z. Li, S. Xiong, C. Sievers, Y. Hu, Z. Fan, N. Wei, H. Bao, S. Chen, D. Donadio, and T. Ala-Nissila, Influence of thermostating on nonequilibrium molecular dynamics simulations of heat conduction in solids, *J. Chem. Phys.* **151**, 234105 (2019).
- ⁴² M. A. Simon, S. Martinez-Garaot, M. Pons, and J. G. Muga, Asymmetric heat transport in ion crystals, *Phys. Rev. E* **100**, 032109 (2019).
- ⁴³ Y. Ren, K. Wu, D. F. Coker, and N. Quirke, Thermal transport in model copper-polyethylene interfaces, *J. Chem. Phys.* **151**, 174708 (2019).
- ⁴⁴ A. Dhar and D. Roy, Heat transport in harmonic lattices, *J. Stat. Phys.* **125**, 801 (2006).
- ⁴⁵ L. G. C. Rego and G. Kirczenow, Quantized thermal conductance of dielectric quantum wires, *Phys. Rev. Lett.* **81**, 232 (1998).
- ⁴⁶ D. Segal, A. Nitzan, and P. Hänggi, Thermal conductance through molecular wires, *J. Chem. Phys.* **119**, 6840 (2003).
- ⁴⁷ D. Segal and A. Nitzan, Spin-boson thermal rectifier, *Phys. Rev. Lett.* **94**, 034301 (2005).
- ⁴⁸ E. Pereira, Thermal rectification in classical and quantum systems: Searching for efficient thermal diodes, *Europhys. Lett.* **126**, 14001 (2019).
- ⁴⁹ Note that the Langevin equation corresponds to Ohmic baths⁵⁰ with the self energies $\Sigma_{1,N}(\omega) = i\omega\gamma_{1,N}$ ⁸.
- ⁵⁰ M. E. Tuckerman, *Statistical Mechanics: Theory and Molecular Simulation*, Oxford University Press, 2010.
- ⁵¹ K. A. Velizhanin, M. Thoss, and H. Wang, Meir-Wingreen formula for heat transport in a spin-boson nanojunction model, *J. Chem. Phys.* **133**, 084503 (2010).
- ⁵² A. Brünger, C. L. Brooks, and M. Karplus, Stochastic boundary conditions for molecular dynamics simulations of ST2 water, *Chem. Phys. Lett.* **105**, 495 (1984).
- ⁵³ E. Vanden-Eijnden and G. Ciccotti, Second-order integrators for Langevin equations with holonomic constraints, *Chem. Phys.* **429**, 310 (2006).
- ⁵⁴ D. J. Evans, E. G. D. Cohen, and G. P. Morriss, Probability of second law violations in shearing steady state, *Phys. Rev. Lett.* **71**, 2401 (1993).
- ⁵⁵ W. Wang and R. D. Skeel, Analysis of a few numerical integration methods for the Langevin equation, *Mol. Phys.* **101**, 2149 (2003).
- ⁵⁶ M. Terraneo, M. Peyrard, and G. Casati, Controlling the energy flow in nonlinear lattices: A model for a thermal rectifier, *Phys. Rev. Lett.* **88**, 094302 (2002).
- ⁵⁷ B. Li, L. Wang, and G. Casati, Thermal diode: Rectification of heat flux, *Phys. Rev. Lett.* **93**, 184301 (2004).

- ⁵⁸ B. Hu, L. Yang, and Y. Zhang, Asymmetric heat conduction in nonlinear lattices, *Phys. Rev. Lett.* **97**, 124302 (2006).
- ⁵⁹ G. T. Craven and A. Nitzan, Upside/Downside statistical mechanics of nonequilibrium Brownian motion. I. Distributions, moments, and correlation functions of a free particle, *J. Chem. Phys.* **148**, 044101 (2018).
- ⁶⁰ G. T. Craven, R. Chen, and A. Nitzan, Upside/Downside statistical mechanics of nonequilibrium Brownian motion. II. Heat transfer and energy partitioning of a free particle, *J. Chem. Phys.* **149**, 104103 (2018).
- ⁶¹ M. Ramm, T. Pruttivarasin, and H. Häffner, Energy transport in trapped ion chains, *New J. Phys.* **16**, 063062 (2016).
- ⁶² M. Tamura, T. Mukaiyama, and K. Toyoda, Quantum walks of a phonon in trapped Ions, *Phys. Rev. Lett.* **124**, 200501 (2020).
- ⁶³ A. C. Barato and U. Seifert, Thermodynamic Uncertainty Relation for Biomolecular Processes, *Phys. Rev. Lett.* **114**, 158101 (2015).
- ⁶⁴ A. Dechant and S.-i. Sasa, Entropic bounds on currents in Langevin systems, *Phys. Rev. E* **97**, 062101 (2018).
- ⁶⁵ S. Saryal, H. Friedman, D. Segal, and B. K. Agarwalla, Thermodynamic uncertainty relation in thermal transport, *Phys. Rev. E* **100**, 042101 (2019).
- ⁶⁶ D. Segal, Thermal conduction in molecular chains: Non-Markovian effects, *J. Chem. Phys.* **128**, 224710 (2008).
- ⁶⁷ Y. Zhou and D. Segal, Interface effects in thermal conduction through molecular junctions: Numerical simulations, *J. Chem. Phys.* **133**, 094101 (2010).
- ⁶⁸ D. Segal, Absence of thermal rectification in asymmetric harmonic chains with self consistent reservoirs: An exact analysis, *Phys. Rev. E* **79**, 012103 (2009).